

Assumption-free fidelity bounds for hardware noise characterization

Nicolo Colombo*

April 10, 2025

Abstract

In the Quantum Supremacy regime, quantum computers may overcome classical machines on several tasks if we can estimate, mitigate, or correct unavoidable hardware noise. Estimating the error requires classical simulations, which become unfeasible in the Quantum Supremacy regime. We leverage Machine Learning data-driven approaches and Conformal Prediction, a Machine Learning uncertainty quantification tool known for its mild assumptions and finite-sample validity, to find theoretically valid upper bounds of the fidelity between noiseless and noisy outputs of quantum devices. Under reasonable extrapolation assumptions, the proposed scheme applies to any Quantum Computing hardware, does not require modeling the device's noise sources, and can be used when classical simulations are unavailable, e.g. in the Quantum Supremacy regime.

1 Introduction

The high potential of Quantum Computing (QC) has not manifested yet in real-world applications (Dasgupta and Humble, 2022). Tasks where QC has proven scalability advantages (Arute et al., 2019) require correcting errors induced by hardware noise. Available Quantum Error Correction algorithms (Lidar and Brun, 2013), based on physics-informed Noise and Error Models (NEMs) that make strong assumptions on the underlying quantum process,

*nicolo.colombo@rhul.ac.uk

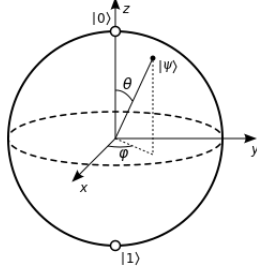


Figure 1: The Bloch sphere represents a qubit, $|\psi\rangle$ as the complex superposition of two states, $|\psi\rangle = \alpha|0\rangle + \beta|1\rangle$, with $\alpha = \cos(\theta/2)$, $\beta = e^{i\phi} \sin(\theta/2)$, $|0\rangle = \begin{bmatrix} 1 \\ 0 \end{bmatrix}$, and $|1\rangle = \begin{bmatrix} 0 \\ 1 \end{bmatrix}$. Measuring a qubit can only produce two outcomes, 0 with probability α^2 and 1 with probability β^2 , and destroys the superposition (by setting either α or β to 0). If the qubit is entangled with another, measuring the first may affect the (unmeasured) state of the second. A quantum circuit consists of a series of matrix operators acting on $|\psi\rangle$ before it is measured.

are computationally expensive and become unreliable for deep circuits, i.e. circuits with many qubits. Existing Machine Learning (ML) methods to improve them (Harper et al., 2020; Canonici et al., 2024) often rely on unverifiable assumptions, e.g. the specific type of quantum noise affecting the device (Google, 2023; Van Den Berg et al., 2023; Rajeev, 2024; McEwen et al., 2022; Thorbeck et al., 2023). They also depend on the model architecture and training (Nguyen et al., 2021; Tindall et al., 2024; Patra et al., 2024) and have theoretical success guarantees only in the limit of infinite samples (Zheng et al., 2023). Uncertainty estimation methods like Caro et al. (2022) or Park and Simeone (2023) mostly focus on Quantum ML applications and can be hardly extended to more general tasks. In particular, it is unclear whether such Quantum ML approaches can directly estimate the output of a given s -qubit quantum device, which is a multivariate discrete distribution over $\mathcal{Y} = \{0, 1\}^s$. Using black-box ML methods for data-driven characterizations of QC hardware noise is a relatively new but promising idea. Martina et al. (2022) and Canonici et al. (2024) show that quantum noise is rich enough to provide a unique fingerprint of a QC machine. The result is obtained from real hardware data but for small circuits (4 qubits). Does the provided noise characterization still hold when the size of the circuits increases, e.g. when s crosses the boundary of the so-called Quantum

Supremacy regime (Preskill, 2012)? And can the characterization be used to provide statistically sound upper bounds for the quantum noise of classically intractable quantum hardware?

Conformal Prediction (CP) is a data-driven, scalable, and assumption-free uncertainty quantification technique. CP’s recent popularity relies on the increasing demand for trustworthy and reliable AI, with general applicability and mild assumptions. Designed and commonly used to assess the uncertainty of ML systems in the finite-sample regime, CP is rarely exploited in AI-unrelated applications, e.g. to calibrate and characterize physical devices or complex natural processes. In principle, CP’s model-agnosticism may help quantify the output randomness of any partially observed physical system. Compared to more standard statistical approaches, e.g. Bayesian inference, CP can be expected to be more robust because it does not require to guess or approximate the system’s dynamics. In QC, modeling the details of the data-generating process is particularly hard because of the unavoidable interactions with the environment and the complex-valued formalism of Quantum Mechanics, which is partially incompatible with the classical notion of probability (Feynman et al., 1951). Can a frequentist approach as CP overcome this challenge?

Using CP to evaluate the unmodeled parts of quantum hardware noise, we provide reliability guarantees for classically intractable QC systems. Technically, we aim to test whether noise characterizations trained on small devices can be *extrapolated* to devices and tasks that go beyond the Quantum Supremacy boundary. Assuming hardware noise increases as a function of a device’s features, e.g. its size and depth, we analyze the validity and efficiency of CP intervals when we calibrate and test the algorithm on circuits of different sizes. A priori, usual CP validity is not guaranteed in this case because the output distributions of small and large devices may be non-exchangeable.

1.1 Contribution

CP for physical systems. Using CP beyond the evaluation of AI systems is new. To our knowledge, there are no examples of CP-based schemes to directly estimate and quantify the uncertainty of physical systems.

Unpaired samples. Park and Simeone (2023) use CP in the QC framework but focus on Quantum ML applications, which are trained to solve standard ML tasks, e.g. MNIST digit recognition. Unlike Park and Simeone

(2023), the noisy and noise-free outputs considered here are associated with the *predictions* and *labels* of a standard ML task because they are unpaired. Except for Hu and Lei (2024), the problem of evaluating unpaired samples, often referred to as the 2-sample problem, has not been addressed in the CP literature. Hu and Lei (2024), likely the only existing work applying CP to a two-sample task, focuses on hypothesis testing for conditional distributions. Our conceptual framework and ratio-based conformity score are similar but allow us to estimate continuous quantities (instead of a binary decision rule) and establish a clear link between the density-ratio conformity score and the target distribution divergences. Moreover, we focus on a specific case of conditional distributions where a heuristic ordering of the object space can be established in terms of a device’s size and depth.

Non-exchangeability. In a QC real-world application, the outputs of classically tractable and intractable devices may be statistically different. As we focus on small quantum machines when we train and calibrate the CP algorithms and intractable systems at test time, calibration and test sets are not exchangeable in our application. Non-exchangeability issues have been widely addressed in the CP literature (Barber et al., 2023). We propose two conceptually different new approaches inspired by the two common strategies used in CP to mitigate distribution shifts, sample reweighting (Boström and Johansson, 2020; Guan, 2023) and calibration training (Papadopoulos et al., 2008; Colombo and Vovk, 2020; Colombo, 2024). The proposed approaches are general and apply to any situations where training, calibration, and test sets come from different realizations of a smooth multivariate meta-distribution, e.g. when $P(Y|X = x) \neq P(Y|X = x')$.

Sample reweighting. In the QC setup, non-exchangeability can be expected to vary as a function of specific feature summaries, e.g. the classical computational complexity required to simulate a system. Our first mitigation approach consists of selecting training and calibration samples after ranking the data according to their complexity. The strategy can be viewed as an extreme application of the Mondrian CP algorithm of Boström and Johansson (2020). In particular, it is different from the distribution drift setup, e.g. Gibbs and Candes (2021), where predictions become increasingly accurate as time passes (allowing asymptotic regret bounds). We show how choosing the ranking function and a threshold reduces the expected undercoverage of

the prediction intervals.

Calibration training. Papadopoulos et al. (2008) proposed to rescale the conformity scores with a pre-trained function of the inputs. While CP-aware training of the prediction model has become common in the literature Colombo and Vovk (2020); Anthony (2020); Stutz et al. (2021), trainable conformity scores have been less explored. In our scheme, we train a shift function that automatically compensates for the distribution drift. Under idealized assumptions, we show that training the shift model reduces the total variation between calibration and test distributions, which is proportional to the validity gap defined in Barber et al. (2023).

A general scheme. The proposed procedure applies beyond the QC framework and can quantify the accuracy of image and text generation models, where the output is also high-dimensional and possibly discrete. Existing CP schemes in the image-generation framework are restricted to image-reconstruction tasks, where CP can be applied pixel-wise by comparing the model output and the original pixels. Bounding the overall distribution distance overcomes this limitation. Moreover, our approach does not require designing expansive multiple-output CP approaches like Messoudi et al. (2021).

1.2 Related Work

CP for generative models Our work is related to the problem of applying CP to multivariate generative models for two reasons: i) The output space is high-dimensional. ii) The predictor is an analytically unavailable *generative distribution* from which we can only sample. Campos et al. (2024) review recent CP approaches for Large Language Models. Kutiel et al. (2023) focus on visualization and use image masks to represent the uncertainty of an image regressor model. Belhasin et al. (2023) attempt to capture spatial correlations when computing CP per-pixel intervals but restrict to image restoration applications. We are unaware of approaches combining CP and the divergence measures used to train generative models, e.g. the Frechet Inception Distance (FID) or Kernelized Wasserstein divergence. A combination of density ratio estimation and CP has appeared in Tibshirani et al. (2019) and Hu and Lei (2024).

Paired and unpaired samples Our approach is related to CP under random effects Dunn et al. (2018). Similar to here, CP intervals are obtained from the samples of an underlying black-box generator but are not explicitly related to distribution distances. Ghosal and Matabuena (2023) provide a conformal algorithm for when the inputs and outputs are distributions. In their setup, however, each sample corresponds to a label, i.e. attributes and labels are paired. Outside the CP framework, techniques to address the 2-sample problem have been proposed in the statistical literature since 1939 (Smirnov, 1939) and mostly in the non-parametric framework (Gretton et al., 2012). The only connection between CP and 2-sample tasks is a recent work on hypothesis testing (Hu and Lei, 2024) (see Section 1.1 for a technical comparison).

CP for QC In QC, CP has been used only in Park and Simeone (2023), which is a direct application of Probabilistic CP Wang et al. (2022). In Park and Simeone (2023), the multiple-output setup is avoided because high-dimensional observables can be handled by performing several separate measurements Caro et al. (2022). The argument in Caro et al. (2022) relates to the generalization properties of Quantum ML algorithms. It is unclear whether this is a more fundamental property of Quantum Computing devices.

Quantum Error Mitigation The problem of hardware noise is handled with QEM (Cai et al., 2023). Machine Learning (ML) methods have been used for QEM since 2020. Unlike us, ML-QEM often focuses on inferring distribution summaries, depends on the underlying error models and requires changing the target circuit (Harper et al., 2020; Liu and Zhou, 2020; Strikis et al., 2021; Wang et al., 2022; Canonici et al., 2024; Adeniyi and Kumar, 2025).

2 Methods

2.1 The Bhattacharyya Coefficient (BC)

The output of small QC hardware can be reproduced using classical computers, i.e. a *simulator* where all quantum operations are noise-free. In this

case, we can compare the noisy outcomes of the hardware with the corresponding ideal output. Let the ideal and noisy outputs be $Y_m \in \{0, 1\}^s$ and $\hat{Y}_m \in \{0, 1\}^s$, where s is the number of measured qubits and $m = 1, \dots, M_{shots}$ indexes a single execution (shot) of the quantum machine.¹ Y_m and \hat{Y}_m can only take binary real values because a qubit collapses into a $\{0, 1\}$ when it is measured. When s qubits of a circuit are measured the noisy and ideal outputs are a series of binary strings, interpreted as i.i.d. draws from two underlying multivariate distributions, P_Y and $P_{\hat{Y}}$, with support $\{0, 1\}^s$. As the noisy device and the classical simulator run independently, there is no relationship between single samples from P_Y and $P_{\hat{Y}}$. For simplicity, we use the same index for the samples from \hat{P}_Y and $P_{\hat{Y}}$, even if a realization of Y_m is *not* the *label* of a realization of \hat{Y}_m . In this setup, hardware noise is proportional to any distribution distance between P_Y and $P_{\hat{Y}}$.

The *fidelity* of two quantum states is a quantification of their similarity, defined as the probability of identifying one state as the other. Its classical counterpart, for discrete random variables, is the Bhattacharyya Coefficient (Bhattacharyya, 1946),

$$\text{BC}(Y, \hat{Y}) = \sum_{y \in \mathcal{Y}} \sqrt{P_Y(y)P_{\hat{Y}}(y)} \quad (1)$$

The BC is related to the Hellinger distance,

$$d_{\text{H}}^2(Y, \hat{Y}) = \frac{1}{2} \sum_{y \in \mathcal{Y}} \left(\sqrt{P_Y(y)} - \sqrt{P_{\hat{Y}}(y)} \right)^2$$

and the Total Variation distance,

$$d_{\text{TV}}(Y, \hat{Y}) = \sum_{y \in \mathcal{Y}} \|P_Y(y) - P_{\hat{Y}}(y)\| \quad (2)$$

In particular, $1 - \text{BC} = d_{\text{H}}^2 \leq d_{\text{TV}} \leq \sqrt{2} d_{\text{H}}$. Inequalities involving the Kullback–Leibler divergence, $d_{\text{KL}} = \text{E}P_{\hat{Y}} \log \frac{P_Y}{P_{\hat{Y}}}$, can be found in (Sason, 2015).

¹ Y_1, \dots, Y_M and $\hat{Y}_1, \dots, \hat{Y}_M$ should be treated as random variables because of the intrinsic Quantum Mechanics non-determinism.

2.2 Large-scale devices

A qubit can assume a dense infinity of states (all points in the Bloch sphere represented in Figure 1) and is described by a complex-valued wave function, ψ , usually encoded as a vector in an infinite-dimensional Hilbert space. Simulating a quantum circuit requires computing the transformations induced by the circuit’s logical gates on ψ . Classical simulations become infeasible when the number of interacting qubits in the circuit increases. The *Quantum Supremacy regime* is defined by the set of tasks that can only be completed in finite time by quantum devices, i.e. would have nearly infinite complexity on a classical machine (Preskill, 2012). Current quantum computers are far beyond this limit (DeCross et al., 2024). Intuitively, however, the boundary has no physical meaning and depends only on the available (classical) computational power compared with the circuit’s complexity, depth, and size, i.e. the number of interacting qubits. This argument justifies

Assumption 2.1. *A quantum system’s behavior may depend on its physical features, the environment in which is run, and its initial state, but not on whether it can be simulated on a classical machine.*

The requirement informally guarantees we can extrapolate a device noise characterization across the boundaries Quantum Supremacy regime. Under Assumption 2.1 we can model the noisy output of a QC device as

$$\hat{Y} \sim Y + \varepsilon_{noise}(Z), \quad Z = \phi(\hat{Y}) \quad (3)$$

where $Z \in \mathcal{Z}$ is a general set of features describing the device and can be extracted from $P_{\hat{Y}}$ through a suitable feature map, ϕ . If ε_{noise} is smooth enough Buriticá and Engelke (2024), we can use ML to *extrapolate* the gap between the ideal and noisy outputs of a classically intractable device by comparing the ideal and noisy outputs of smaller devices. In practice, knowing or modeling the physical data-generating process underlying (3) is challenging, especially because ε_{noise} depends on partly unpredictable interactions between a quantum machine and the environment or the hardware defects. In this sense, black-box ML systems like CP are ideal because they rely on minimal assumptions and apply to any black-box input-output system. Assuming $\varepsilon_{noise}(Z) = \varepsilon_0 g(Z)$, where ε_0 depends on the quantum machines where the circuit is run but not on the circuit size, we show how to adapt a standard Split-CP algorithm to produce prediction intervals that are valid even when calibration and test set do not come from the same distribution.

2.3 Empirical BC approximation

The dimensionality of the n -th distribution’s support, s_n , is the number of qubits measured in the n -th circuit. In Figure 2, $s_n = 2$ because only q_2 and q_3 are measured. As the number of qubit measurements grows, e.g. for $d > 5$, computing the BC explicitly becomes expansive or unfeasible because of the sum over all possible output configurations, $\sum_{y \in \mathcal{Y}_n} \sim O(2^{s_n})$. Moreover, the explicit form of the distribution densities, $P_{\hat{Y}}$ and P_Y , is usually unknown and depends on the quantum dynamics of the qubits inside the circuit with and without hardware noise. While Quantum Mechanics and the circuit layout may be used to obtain a theoretical estimate of P_Y , modeling $P_{\hat{Y}}$ would require including system-specific Noise Error Models for all device disturbances. A data-driven option is to estimate the densities from the available samples using flexible enough ML algorithms, e.g. deep models or Kernel Density Estimation (KDE). Nonparametric estimators like KDE are assumption-free but rely on the careful choice of the bandwidth and become unstable in high dimensions. Parametrized models, e.g. Neural Networks, may be misspecified and never capture substantial details of the distributions (even for an infinite sample size). Our estimation strategy is hyperparameter-free and independent from the dimensionality of the distribution support. The idea is to replace straightforward density estimations with a more constrained but stable density-ratio estimation Sugiyama et al. (2012). The need to estimate a density ratio is shared with other works, e.g. Tibshirani et al. (2019) or Hu and Lei (2024), and is closely related to CP conditional validity (see Section 2.5 for more details). Our motivation for using a density-ratio estimator comes from a direct manipulation of the conformity score, $A = \text{BC}(Y, \hat{Y})$. More explicitly,

$$\text{BC} = \sum_{y \in \mathcal{Y}} \sqrt{P_Y(y)P_{\hat{Y}}(y)} = \sum_{y \in \mathcal{Y}} P_{\hat{Y}}(y) \sqrt{\frac{P_Y(y)}{P_{\hat{Y}}(y)}} \quad (4)$$

$$\sim \frac{1}{M_{shots}} \sum_{m=1}^{M_{shots}} \sqrt{\frac{p_Y(\hat{Y}_m)}{p_{\hat{Y}}(\hat{Y}_m)}} = E_{\hat{Y}} \sqrt{\hat{r}(\hat{Y})} \quad (5)$$

where $\hat{r}(\hat{Y}) \sim \frac{p_Y(\hat{Y}_m)}{p_{\hat{Y}}(\hat{Y}_m)}$ is an empirical estimation of the ratio between the two densities evaluated and $E_{\hat{Y}}(\hat{r}(\hat{Y}))$ its empirical expectation obtained from the available noisy samples, $\{Y_{n1}, \dots, Y_{nM_{shots}}\}$. We refer to Sugiyama et al.

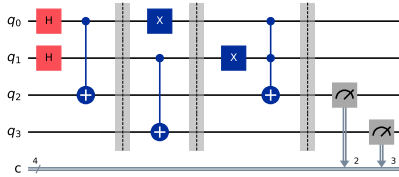


Figure 2: The modular 4-qubit quantum circuit of Martina et al. (2022). The 3-gate structure is repeated 3 times to increase the circuit depth. The top horizontal lines and blocks represent the device’s interacting qubits and logical gates. The bottom line represents the device output. In this case, only 2 qubits are measured, q_2 and q_3 , making each run produce a 2-digit binary string, e.g. $Y_m, \hat{Y}_m \in \{00, 01, 10, 11\}$. The first two blue 2-qubit links represent CNOT gates and the third 3-qubit is a Toffoli gate. See Barenco et al. (1995) for a formal definition. The red boxes are Hadamard gates, used to prepare the unobserved qubits into an equal superposition state $\frac{1}{2}(|0\rangle + |1\rangle)$. By convention, the initial state of all qubits is $|0\rangle$. The grey vertical lines represent 4-qubit synchronization.

(2012) for a review of the theoretical and empirical advantages of estimating \hat{r} instead of the two densities separately.

2.4 Conformal upper bounds

Assume we have a set of N classically tractable circuits and run them on a given QC machine. Let $n = 1, \dots, N$ index these N circuits and $m = 1, \dots, M_{shots}$ the i.i.d. measurements from each circuit, i.e. the execution outputs, and Y_{nm} and \hat{Y}_{nm} the m -th noiseless and noisy measurements obtained from the n -th circuit. As the dimensionality of a circuit’s output depends on the number of measurements, we do not require Y_{nm} and $Y_{n'm}$ to have the same dimensionality. For example, we may have $Y_{nm} \in \{0, 1\}^{s_n}$ and $Y_{n'm} \in \{0, 1\}^{s_{n'}}$ with $s_n \neq s_{n'}$. Naturally, we require different runs from the same circuit to have the same dimensionality, i.e. $Y_{nm} \in \{0, 1\}^{s_n}$ for all $m = 1, \dots, M_{shots}$.

Let $N + 1$ index a test circuit that we can only run on the noisy device and $\hat{P}_{\hat{Y}_{N+1}}$ the corresponding output distribution. The prediction interval

on the BC between \hat{Y}_{N+1} and Y_{N+1} produced by a Split-CP algorithm is an upper bound obeying

$$\text{Prob} \left(\text{BC}(Y_{N+1}, \hat{Y}_{N+1}) \geq Q_\alpha \right) \geq 1 - \alpha \quad (6)$$

$$Q_\alpha = \sup_q \left\{ \sum_{n=1}^N \mathbf{1}(\text{BC}(Y_n, \hat{Y}_n) \geq q) \geq n_\alpha \right\} \quad (7)$$

$$n_\alpha = \lceil (1 - \alpha)(N + 1) \rceil \quad (8)$$

The bound *marginal validity* holds when the data generating distribution of the calibration and test sets, $\{(Y_n, \hat{Y}_n)\}_{n=1}^N$ and (Y_{N+1}, \hat{Y}_{N+1}) , are exchangeable. In this case, (6) is guaranteed by the definition of the empirical quantile of exchangeable samples. See Lemma 1 of Tibshirani et al. (2019) for a simple proof of the quantile lemma and Vovk et al. (2005) or Angelopoulos and Bates (2021) for a smooth introduction to CP.

Central to any CP algorithm is a scoring function, or *conformity score*, A , which measures the quality of an output given the corresponding label. In our case,

$$A_n = \text{BC}(\hat{Y}_n, Y_n), \quad n = 1, \dots, N \quad (9)$$

In practice, (6) is obtained by finding an upper bound for $A_{N+1}(Y) = \text{BC}(\hat{Y}_{N+1}, Y)$, where Y represent any s_{N+1} - dimensional random variable within distance Q_α from the unknown ideal output, Y_{N+1} .

2.5 BC conformal extrapolation

Let Z_1, \dots, Z_N and Z_{N+1} be the features of N quantum circuits that can be simulated on a classical machine and a large circuit that can not. The N tractable circuits are run on quantum hardware and a classical simulator to produce \hat{Y}_{nm} and Y_{nm} , where $n = 1, \dots, N$ and $m = 1 \dots, M_{shots}$. The $N + 1$ -th circuit can not be simulated classically but can be run on the quantum hardware to obtain $\hat{Y}_{(N+1) m}$, $m = 1 \dots, M_{shots}$. As the $(N+1)$ -th circuit may be much more noisy than the others the conformity scores $A_n = \text{BC}(Y_n, \hat{Y}_n)$, $n = 1, \dots, N$ and $A_{N+1} = \text{BC}(Y_{N+1}, \hat{Y}_{N+1})$ may be non-exchangeable. In

this case, (6) does not hold and should be replaced by (Barber et al., 2023)

$$\text{Prob}\left(\text{BC}(Y_{N+1}, \hat{Y}_{N+1}) \geq Q_\alpha\right) \geq 1 - \alpha - \text{gap} \quad (10)$$

$$\text{gap} = \frac{1}{N+1} \sum_{n=1}^N d_{\text{TV}}(A_n, A_{N+1}) \quad (11)$$

$$Q_\alpha = \sup_q \left\{ \sum_{n=1}^N \mathbf{1}(A_n \geq q) \geq \lceil (1 - \alpha)(N + 1) \rceil \right\} \quad (12)$$

$$A_n = \text{BC}(Y_n, \hat{Y}_n) \quad (13)$$

The practical use of the bound is limited because we cannot estimate $d_{\text{TV}}(A_n, A_{N+1})$, $n = 1, \dots, N$, without knowing all noise sources of the test device or having samples from the noiseless outputs, Y_{N+1} . Two orthogonal general strategies have been proposed to mitigate similar non-exchangeability issues, sample reweighting, e.g. the Mondrian Conformal Prediction algorithm of Boström and Johansson (2020) and the localization approaches of Tibshirani et al. (2019) and Guan (2023), and calibration training, where the calibration score function is trained to account for possible object-conditional variability.² These and follow-up works focus on establishing CP-conditional validity instead of addressing general shifts between the calibration and test distributions. Replacing CP marginal validity (6) with an exact or approximate input-conditional version of it is challenging and, in general, practically unachievable (Vovk, 2012). Assuming there exists a feature map, $Z = \phi(\hat{Y}) \in \mathcal{Z}$, defined for any \hat{Y} , i.e. for any QC device, estimating an upper bound of the BC between the noisy and noiseless outputs of classically intractable circuits would be equivalent to finding a quantile function $Q : \mathcal{Z} \otimes (0, 1) \rightarrow [0, 1]$, such that

$$\text{Prob}\left(\text{BC}(Y_{N+1}, \hat{Y}_{N+1}) \geq Q(z, \alpha) | Z_{N+1} = z\right) \geq 1 - \alpha \quad (14)$$

where $Z_n = \phi(\hat{Y}_n)$ are the features of the n -th device. In particular, (14) would automatically provide valid noise quantification for large devices by setting $z = Z_{N+1}$ at test time. In the Quantum Supremacy regime, however, this is impossible because circuits with $z = Z_{N+1}$ are classically intractable

²The latter approach was initiated by Papadopoulos et al. (2008) in 2008 but has been rarely exploited fully or investigated further. See Colombo (2024) for a more recent example.

and cannot be used to calibrate the intervals. More generally, estimating the empirical quantile of the conditional distribution for any $z \in \mathcal{Z}$ when $\mathcal{Z} \subseteq \mathbb{R}^d$ is impossible if $N < \infty$ because the probability of having N samples with $z = Z_{N+1}$ in the calibration set is zero. (Vovk, 2012). Here we focus on our specific setup and approximate conditional validity based on two observations

1. We may be able to extract from \hat{Y} an *ordinal feature*, $S = \phi(\hat{Y})$, such that

$$d_{\text{TV}}(BC_n, BC_{n'}) \propto f(|S_n - S_{n'}|), \quad S_n = \phi(\hat{Y}_n), \quad \partial_t f(t) > 0 \quad (15)$$

For example, S may be a weighted sum of a circuit’s depth and number of interacting qubits.

2. Since the object attributes are distributions, we can infer an arbitrarily high-dimension feature map, $\phi(\hat{Y}) \in \mathbb{R}^q$, such that $BC(Y_n, \hat{Y}_n) \approx w^T \phi(\hat{Y})$ obeys

$$\tilde{A}(\hat{Y}) = BC(Y, \hat{Y}) - w^T \phi(\hat{Y}) \sim P_{\tilde{A}} \quad \text{for all } \hat{Y} \quad (16)$$

for some $w \in \mathbb{R}^q$

We formalize these assumptions to derive two non-exchangeability mitigation algorithms in Sections 2.5.1 and 2.5.2. In the experiments, we combine the algorithms and test them empirically against a baseline CP algorithm, i.e. the standard Split CP approach without non-exchangeability mitigation.

2.5.1 Sample selection with an ordinal feature

The idea is to rank the calibration samples according to an ordinal feature extracted from the output distributions. Assuming the test samples rank higher, we show that discarding low-rank calibration samples may reduce the validity gap in (10). In this section, we make the following

Assumption 2.2. *Let Y, \hat{Y} and Y', \hat{Y}' be any two noiseless and noisy distributions of two devices, $A = BC(Y, \hat{Y})$, and $A' = BC(Y', \hat{Y}')$. There exists a one-dimensional score, $\phi(\hat{Y}) \in \mathbb{R}_+$, such that the Total Variation distance between A and A' obeys*

$$d_{\text{TV}}(A, A') \propto |\phi(\hat{Y}) - \phi(\hat{Y}')| \quad (17)$$

³More formally, \tilde{A} is such that the joint distribution of \tilde{A} and \hat{Y} factorizes, that is $P_{\tilde{A}\hat{Y}} = P_{\tilde{A}}P_{\hat{Y}}$

Under this assumption, we can prove the following

Lemma 2.3. *Let $S_n = \phi(\hat{Y}_n)$, $n = 1, \dots, N + 1$ be defined as in Assumption 2.2 and assume $BC(Y_n, \hat{Y}_n) \sim \mathcal{N}(S_n, 1)$ for all $n = 1, \dots, N + 1$ with $S_n = s_1$ for $n = 1, \dots, \bar{n}$, $S_n = s_2 > s_1$ for $n = \bar{n} + 1, \dots, N$, and $S_{N+1} = s_3 > s_2$. Then, if $|s_3 - s_1| < \frac{1}{40}$, and*

$$|s_3 - s_1| > \frac{N - n}{N - \bar{n} + 1} |s_2 - s_1| \quad (18)$$

the validity gap defined in (10) is reduced by discarding the first \bar{n} samples.

Proof of Lemma 2.3 Let $A_n = BC(Y_n, \hat{Y}_n)$, $n = 1, \dots, N + 1$. Under the Lemma assumptions, the validity gap of Barber et al. (2023) becomes

$$\text{gap} = \frac{\sum_{n=1}^N w_n d_{TV}(A_n, A_{N+1})}{1 + \sum_{n=1}^N w_n} = \frac{\gamma \bar{n} |s_1 - s_3| + (N - \bar{n}) |s_2 - s_3|}{2(N + 1)} \quad (19)$$

where $\gamma = \frac{1}{5}$ as shown in Devroye et al. (2018). The claim is obtained by requiring

$$\frac{\bar{n}}{N + 1} |s_1 - s_3| + \frac{\bar{n}}{N + 1} |s_2 - s_3| < \frac{N - \bar{n}}{N - \bar{n} + 1} |s_1 - s_2| \quad (20)$$

□

In the experiments, we let $S_n = s(Z_n)$ be the number of qubits in the n -th circuit, $n = 1, \dots, N + 1$ and assume the total variation distance between the corresponding BCs grows linearly in $|S_n - S_{n'}|$. In this case, the validity gap can be reduced if

$$\frac{\sum_{n=1}^N |S_n - S_{N+1}|}{1 + N} > \min_{s_{min} \in \mathbb{R}} \frac{\sum_{n=1}^N \mathbf{1}(S_n > s_{min}) |S_n - S_{N+1}|}{1 + \sum_{n=1}^N \mathbf{1}(S_n > s_{min})} \quad (21)$$

While searching for $s_{min} \in \mathbb{R}$ requires trying $N + 1$ values and is always feasible, s_{min} is not guaranteed to fulfil (21) if the range of available circuit sizes is limited, however. In our experiments, we let s_{min} be the second largest circuit size in the calibration set. Calibration samples associated with smaller sizes are discarded or used to fit the shift model described in the next paragraph.

2.5.2 Calibration training

More explicit guarantees can be obtained under

Assumption 2.4. Let $\hat{Y}_m \sim P_{\hat{Y}}$ and $Y_m \sim P_{\hat{Y}}$, $m = 1 \dots, M$, be the noisy and noiseless i.i.d. outputs of a QC device and $\hat{BC}(Y, \hat{Y})$ the corresponding empirical estimation of (1). Then, for any \hat{Y} and Y , there exists a scalar function, $bc = bc(\hat{Y})$, that approximates $\hat{BC}(Y, \hat{Y})$ and obeys

$$\varepsilon_{BC} = |bc(\hat{Y}) - \hat{BC}(Y, \hat{Y})| \perp\!\!\!\perp (\hat{Y}, Y) \quad (22)$$

i.e. has attribute-independent residuals.

In this case, we can prove the following

Theorem 2.5. Let \hat{BC} and bc be as in Assumption 2.4, $\hat{Y}_{nm} \sim P_{\hat{Y}_n}$ and $Y_{nm} \sim P_{\hat{Y}_n}$, $n = 1, \dots, N + 1$, $m = 1 \dots, M$, be the noisy and noiseless outputs of $N + 1$ QC devices, and \hat{BC}_n , $n = 1, \dots, N$, the associated empirical estimation of (1). Then, for any $t > 0$ and any $\alpha \in (0, 1)$,

$$\text{Prob} \left(BC(Y_{N+1}, \hat{Y}_{N+1}) \geq bc(\hat{Y}_{N+1}) - q_\alpha - t \right) \geq (1 - \alpha)(1 - 2e^{-\frac{2t^2}{C_{N+1}}}) \quad (23)$$

$$q_\alpha = \inf_q \left\{ \sum_{n=1}^N \mathbf{1} \left(|\hat{BC}_n - bc(Y_n, \hat{Y}_n)| < q \right) \geq \lceil (1 - \alpha)(N + 1) \rceil \right\} \quad (24)$$

where $C_{N+1} = |c_{N+1} - c_{N+1}^{-1}|$, $c_{N+1} = \sqrt{\min\{\min_y P_{Y_n}(y), \min_y P_{\hat{Y}_n}(y)\}}$.

Remark. Assuming there exists a conditional model of a circuit's BC with \hat{Y} -independent residuals is a weaker assumption than assuming the existence of the QEM function ϵ_{noise} in (3).

Proof of Theorem 2.5. By assumption, $|\hat{BC}_n - bc(\hat{Y}_n)|$ are i.i.d. and then exchangeable. The definition of q_α implies

$$\text{Prob} \left(\hat{BC}_{N+1} \geq bc(\hat{Y}_{N+1}) - q_\alpha \right) \geq 1 - \alpha \quad (25)$$

for all $\alpha \in (0, 1)$. For any $n = 1, \dots, N + 1$, $BC(Y_n, \hat{Y}_n)$ is the expectation under $P_{\hat{Y}_n}$ of $R_n(y) = \sqrt{\frac{P_{Y_n}(y)}{P_{\hat{Y}_n}(y)}}$. Hoeffding's inequality bounds the deviation of its

empirical estimation in terms of the number of samples, M , and the variable range with high probability. In particular, we have

$$R_n \in \left[\sqrt{\min_y P_{Y_n}(y)}, \frac{1}{\sqrt{\min_y P_{\hat{Y}_n}(y)}} \right] \subseteq [\sqrt{c_n}, \sqrt{1/c_n}] \quad (26)$$

$$c_n = \min\{\min_y P_{Y_n}(y), \min_y P_{\hat{Y}_n}(y)\} \quad (27)$$

and, for any $t > 0$,

$$\text{Prob} \left(\left| M^{-1} \sum_{m=1}^M \sqrt{\frac{P_{Y_n}(\hat{Y}_{nm})}{P_{\hat{Y}_n}(\hat{Y}_{nm})}} - E_{\hat{Y}_n} R_n(\hat{Y}_n) \right| \leq t \right) = \quad (28)$$

$$= \text{Prob} \left(\left| \hat{B}C_n - BC(Y_n, \hat{Y}_n) \right| \leq t \right) \geq 1 - e^{-\frac{2t^2}{M C_n}} \quad (29)$$

where $C_n = |c_n - c_n^{-1}|$. The statement is then obtained by combining the concentration and CP bounds, (28) and (25). \square The BC approximator needs to be trained on data that are not used to calibrate the CP algorithm. Ideally, the training data set should be a random subset of all available data, but this is not required for the validity of (10). In general, however, the empirical estimation of $bc(\hat{Y})$ will not fulfil Assumption 2.4. If we assume the BC is Gaussian distributed around a conditional mean that depends only on (features extracted from) \hat{Y} , and bc is a good enough approximation of such conditional mean, we do not need Assumption 2.4 to show that using $\tilde{A}_n = |BC(Y_n, \hat{Y}_n) - bc(X_n)|$ instead of $A_n = BC(Y_n, \hat{Y}_n)$ reduces the validity gap.

Lemma 2.6. *Let $BC_n = BC(Y_n, \hat{Y}_n) \sim \mathcal{N}(\mu_n, 1)$, $n = 1, \dots, N + 1$, where the unknown conditional mean depends only on \hat{Y}_n , i.e. $\mu_n = \mu(\hat{Y}_n)$. Let $bc(\hat{Y}_n) \approx E(BC_n | \hat{Y}_n) = \mu_n$ be a pre-trained approximation of the conditional expectation of BC_n . Then replacing $A_n = BC_n$ with $\tilde{A}_n = |BC_n - bc(\hat{Y}_n)|$ in (10) is reduces the validity gap if*

$$\max_n \{|\mu_n - bc(\hat{Y}_n)|\} \leq \frac{1}{5} \frac{1}{N} \sum_{n=1}^N |\mu_n - \mu_{N+1}|, \quad (30)$$

Proof of Lemma 2.6. According to Theorem 1.3 of Devroye et al. (2018), the Total Variation distance between two one-dimensional Gaussians

with unit variance and means μ and μ' obeys

$$\frac{4}{200}|\mu - \mu'| \leq d_{\text{TV}}(\mathcal{N}(\mu, 1), \mathcal{N}(\mu', 1)) \leq \frac{1}{2}|\mu - \mu'| \quad (31)$$

Consider a CP algorithm calibrated using $\tilde{A}_n = BC_n - bc(\hat{Y}_n) \sim \mathcal{N}(\mu_n - bc(\hat{Y}_n), 1)$, $n = 1, \dots, N + 1$, instead of $A_n = BC_n$. In this case, the validity gap defined in (10) obeys

$$\text{g}\tilde{\text{a}}\text{p} = \frac{1}{N + 1} \sum_{n=1}^N d_{\text{TV}}(\tilde{A}_n, \tilde{A}_{N+1}) \quad (32)$$

$$= \frac{1}{N + 1} \sum_{n=1}^N d_{\text{TV}}(\mathcal{N}(\mu_n - bc(\hat{Y}_n), 1), \mathcal{N}(\mu_n - bc(\hat{Y}_n), 1)) \quad (33)$$

$$\leq \frac{1}{N + 1} \frac{1}{2} \sum_{n=1}^N |\mu_n - bc(\hat{Y}_n) - \mu_{N+1} + bc(\hat{Y}_{N+1})| \quad (34)$$

$$\leq \frac{N}{N + 1} \max_n \{|\mu_n - bc(\hat{Y}_n)|\} \quad (35)$$

The validity gap of a CP algorithm calibrated using $A_n = BC_n \sim \mathcal{N}(\mu_n, 1)$ obeys

$$\text{gap} = \frac{1}{N + 1} \sum_{n=1}^N d_{\text{TV}}(A_n, A_{N+1}) \quad (36)$$

$$= \frac{1}{N + 1} \sum_{n=1}^N d_{\text{TV}}(\mathcal{N}(\mu_n, 1), \mathcal{N}(\mu_n, 1)) \quad (37)$$

$$\leq \frac{1}{N + 1} \frac{1}{5} \sum_{n=1}^N |\mu_n - \mu_{N+1}| \quad (38)$$

The latter is larger than $\text{g}\tilde{\text{a}}\text{p}$ if

$$\frac{1}{N} \frac{1}{5} \sum_{n=1}^N |\mu_n - \mu_{N+1}| \geq \max_n \{|\mu_n - bc(\hat{Y}_n)|\} \quad (39)$$

The claim follows from noting that the total variation between two random variables, Z, Z' , is larger than the total variation distance between any function applied to Z and Z' , e.g. between $|Z|$ and $|Z'|$. See the discussion below

Lemma 1 of Barber et al. (2023) for a discussion about the tightness of the bound. \square

After training bc and calibrating a CP algorithm with $|A_n - bc(\hat{Y}_n)|$, the prediction intervals for the BC become

$$C_{N+1} = [bc(\hat{Y}_{N+1}) - q_\alpha, bc(\hat{Y}_{N+1}) + q_\alpha] \quad (40)$$

$$q_\alpha = \inf_q \left\{ \sum_{n=1}^N \mathbf{1}(|BC_n - bc(\hat{Y}_n)| \leq q) \geq \lceil (1 - \alpha)(N + 1) \rceil \right\} \quad (41)$$

and, under the assumptions of Lemma 2.6, have approximate $(1 - \alpha)$ coverage

$$\text{Prob}(BC(Y_{N+1}, \hat{Y}_{N+1}) \in C_{N+1}) \geq (1 - \alpha) - \max_n \{|\mu_n - bc(\hat{Y}_n)|\} \quad (42)$$

In the experiments, we use $bc(Z) = \arg \min_g \mathbb{E} \|A - g(Z)\|^2$, where $Z = (\hat{\mathbb{E}}(\hat{Y}), \hat{\mathbb{E}}(\hat{Y} \otimes \hat{Y}^T))$ are the first and empirical second moments of \hat{Y}_n .

3 Experiments

We ran a synthetic experiment to assess the accuracy of the proposed BC estimator and used simulated and real quantum hardware data to validate the prediction of the CP algorithm. A summary of how we applied the methods described in Section 2.5 in practice is given in the following section 3.1.

3.1 Pipeline

Given a quantum machine, e.g. `ibm_kyiv` at IBM (2025), we proceed as follows.

1. Use the quantum machine to run N classically tractable circuits and collect the corresponding noisy outputs, \hat{Y}_{nm} , $n = 1, \dots, N$ and $m = 1, \dots, M_{shots}$.
2. Use a classical simulator to run the same N circuits and collect the corresponding noise-free outputs, Y_{nm} , $n = 1, \dots, N$ and $m = 1, \dots, M_{shots}$.
3. Compute the BC for all $n = 1, \dots, N$.
4. Split the data set according to the circuit sizes, s_n , e.g. we let $I_{train} = \{n : s_n < s_{max}\}_{n=1}^N$, $s_{max} = \arg \max_n \{s_n\}_{n=1}^N$ and $I_{cal} = \{n : s_n = s_{max}\}_{n=1}^N$.

5. Use $\{\hat{Y}_n, Y_n\}_{n \in I_{train}}$ to train the shift function, $g(\phi(\hat{Y}))$, by minimizing $\sum_{n \in I_{train}} (A_n - g(\phi(\hat{Y}_n)))^2$, where $\phi : P_{\hat{Y}} \rightarrow \mathbb{R}^d$ is an arbitrary feature map.
6. Evaluate the transformed conformity scores, $B_n = \text{BC}(Y_n, \hat{Y}_n) - g(\phi(\hat{Y}_n))$ for all $n \in I_{cal}$.
7. Let Q_α be the $1 - \alpha$ empirical quantile of the calibration scores, $\{B_n\}_{n \in I_{cal}}$.
8. Let \hat{Y}_{N+1} be the noisy output of a classically intractable test circuit and evaluate $g(\phi(\hat{Y}_{N+1}))$.
9. Return the upper bound for the BC between \hat{Y}_{N+1} and its ideal (unavailable) counterpart,

$$\text{BC}(Y_{N+1}, \hat{Y}_{N+1}) \geq g(\phi(\hat{Y}_{N+1}) + Q_\alpha) \quad (43)$$

which hold with probability $1 - \alpha - \text{gap}$, with

$$\text{gap} = 2 \frac{\sum_{n \in I_{cal}} d_{\text{TV}}(A_n - g(\phi(\hat{Y}_n)), A_{N+1} - g(\phi(\hat{Y}_{N+1})))}{|I_{cal}| + 1} \quad (44)$$

$$A_n = \text{BC}(Y_n, \hat{Y}_n) \quad (45)$$

$$\phi(\hat{Y}_n) = (\hat{\text{E}}(\hat{Y}_n), \hat{\text{E}}(\hat{Y}_n \otimes \hat{Y}_n^T)) = \left(\sum_{m=1}^M \hat{Y}_{nm}, \sum_{m=1}^M \hat{Y}_n \otimes \hat{Y}_{nm}^T \right) \quad (46)$$

3.2 Density-ratio estimator

In all experiments, we use a Logistic Regression (LR) parametric estimator for $\hat{r} = \frac{P_Y}{P_{\hat{Y}}}$,

$$\hat{r}_{\text{LR}}(\hat{Y}_n) = \frac{f(\hat{Y}_n)}{1 - f(\hat{Y}_n)}, \quad (47)$$

$$f(Y) = \sigma(\hat{\theta}^T \phi(Y)) \sim \text{Prob}(Y \sim P_Y | Y) \quad (48)$$

where $\theta \in \mathbb{R}^d$, $d \in \mathbb{N}_+$ is an optimized free parameter and $\phi(\hat{Y}_n)$ a fixed feature map from $\{\hat{Y}_{n1}, \dots, \hat{Y}_{nM_{shots}}\}$ to \mathbb{R}^d . Other options include matching all moments of P_Y and $rP_{\hat{Y}}$ under the assumption that the distributions belong to a Reproducing Kernel Hilbert Space (RKHS) (Sugiyama et al., 2012).

3.3 Synthetic data

We generated a set of multivariate Bernoulli product distributions of dimension, with dimensions $s \in \{10, 20, 40, 80\}$ and ground truth and perturbed weights, $w, \hat{w} \in [0, 1]^s$. Ground truth weights, with profile $w_{\log i} \propto \frac{\log(1+i)}{s}$, $w_{rand i} \propto \frac{U * i}{s}$, $U \sim \text{Uniform}[0, 1]$, and $w_{cos i} \propto \cos^2(\frac{\pi}{\epsilon+i})$, $\epsilon = 10^{-4}$, $i = 1, \dots, s$, were perturbed using three different perturbations, $\epsilon_{\log i} \propto \log(\epsilon + w_i)$, $\epsilon_{rand i} = w_i * V$, $V \in \mathcal{N}(0, 1)$, and $\epsilon_{cos i} = \cos(w_i * 2\pi)$. The unspecified proportionality constants guaranteed that all w_i and \hat{w}_i were non-negative and lower than 1. Each ground truth profile was perturbed with all three perturbations. For all (w, \hat{w}) pairs, we estimated the Bhattacharyya distance, $d_{BC} = -\log BC$, the Kullback–Leibler divergence, d_{KL} , and the Total Variation distance, d_{TV} defined in (2), between the associated ground truth and perturbed distributions with the density-ratio estimator of Sections 2.3 and 3.2 and compared them with the theoretical Bhattacharyya distance between two multivariate Bernoulli product distributions,

$$\bar{d}_{BC} = -\log \prod_{i=1}^s \left(\sqrt{w_i \hat{w}_i} + \sqrt{(1-w_i)(1-\hat{w}_i)} \right) \quad (49)$$

In the first run, the highest and lowest BC distances were 1.112 and 0.016, for $w = w_{cos}$, with $\epsilon = \epsilon_{\log}$ and $s = 80$, and $w = w_{\log}$, with $\epsilon = \epsilon_{cos}$ and $s = 10$.

3.4 Simulated data

A *realistic* data set was generated by designing circuits of varying sizes and depths and running them on the IBM *fake backends* and the Qiskit Aer simulator (Qiskit, 2025) to obtain the corresponding noisy and ideal outputs, \hat{Y}_n and Y_n . 36 circuits, called **W-State**, **Portfolio Optimization with VQE**, **Deutsch-Jozsa**, **Graph State**, **GHZ State**, and **Variational Quantum Eigensolver** were generated using the algorithms of Apak et al. (2024) with 6 different sizes $s \in \{5, 7, 9, 11, 13, 15\}$. 12 circuits, called **Random** and **Deep Random**, were generated using the Qiskit random generator with parameters, (`nqubits = s, depth = s`) and (`nqubits = s, depth = 3 * s`), $s \in \{5, 7, 9, 11, 13, 15\}$. 6 additional circuits, all with size 4 but different depths, were generated using the `walker` method of Martina et al. (2022) with depth parameter $s \in \{5, 7, 9, 11, 13, 15\}$. Figure 2 displays an example of a `walker` circuit with depth 3. All circuits were run 5 times on 5

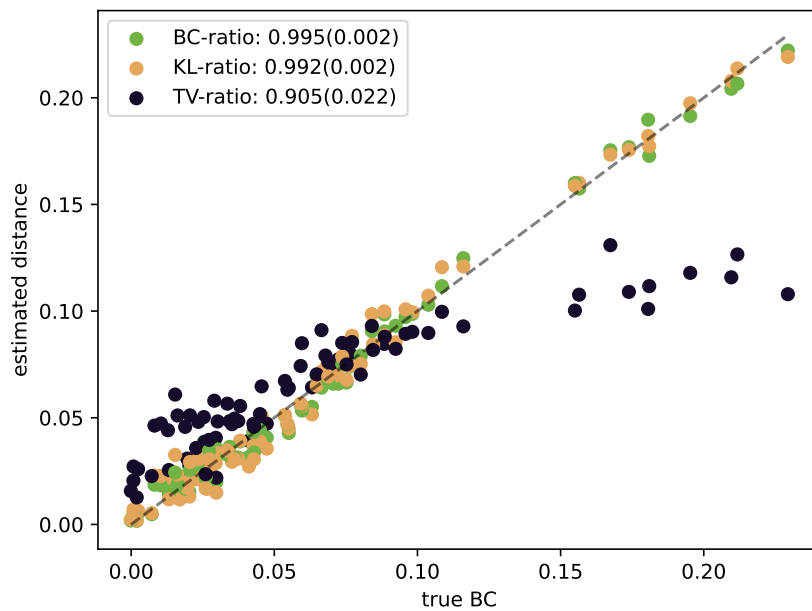


Figure 3: Scatter plot between the theoretical Bhattacharyya distance, \bar{d}_{BC} defined in (49), and the density-ratio estimation of d_{BC} , d_{KL} , and d_{TV} obtained for all weights in the first of 5 simulations. All distances were min-max normalized before computing the correlation. The legend reports the average correlation and corresponding standard deviations on the 5 equivalent runs.

IBM fake backends, `fake_cusco`, `fake_kawasaki`, `fake_kyiv`, `fake_kyoto`, and `fake_osaka`, and using Qiskit Aer simulator. All simulations produced $M_{shots} = 1000$ quantum shots per run. We designed four different setups to test the mitigation strategies of Section 2.5, `all`, `mondrian`, `shift`, and `shift+mondrian`. In `shift+mondrian`, we followed the procedure described in Appendix 3.1, where the shift model, g , was a Scikit-Learn Random Forest regressor with default parameters, $\phi(\hat{Y}) = [E\hat{Y}, \text{vec}(E(\hat{Y} - E\hat{Y}) \otimes (\hat{Y} - E\hat{Y}))]$, and $A \in \{d_{BC}, d_{KL}, d_{TV}\}$. In `all` and `mondrian`, we did not train any shift model and used data from circuits with sizes $s < s_{max} = 15$ (`all`) and $s = s_{2nd\ max} = 13$ (`mondrian`) for calibration. In `shift` and `shift+mondrian`, we trained the shift model on a randomly selected half of all $s < s_{max}$ data (`shift`) and only on $s < s_{2nd\ max}$ data (`shift+mondrian`). In both cases, we let the calibration set contain all the remaining $s < s_{max}$ data. The test set always consisted of all $s = s_{max} = 15$ data. Table 1 shows the average size and coverage of the CP prediction intervals for all setups.

3.5 Real data

Finally, we tested the algorithms on hardware data from Martina et al. (2022). We selected data generated by running 9 modular 4-qubit `walker` circuits of increasing depth on different quantum machines. Figure 2 shows a `walker` circuit of depth 3. The others were obtained by repeating its structure 2 and 3 times (see Martina et al. (2022) for more details). Each circuit ran on 5 different quantum machines, `ibm_athens`, `ibm_casablanca`, `ibm_lima`, `ibm_quito`, and `santiago`, with $M_{shots} = 1000$ quantum shots per execution. The corresponding noise-free data were generated using Qiskit’s Aer simulator (Qiskit, 2025). We followed the procedure described in Appendix 3.1 and considered the same distribution distances and setups of Section 3.4 with s replaced by the circuit depths. The algorithms were all tested on data generated by the deepest circuit (depth = 9). Table 2 shows the average size and coverage of the CP prediction intervals for all setups.

3.6 Discussion

Synthetic data The proposed density-ratio estimation seems to be a good proxy for the theoretical Bhattacharyya distance. The differences between d_{KL} and d_{BC} and d_{TV} for higher levels of noise show that d_{TV} ignores features accounted by the other distances. The strong similarity between d_{KL}

d_{KL} (simulated data)	coverage	size
all	0.9 (0.0136)	1.971 (0.604)
mondrian	0.922 (0.0111)	3.273 (1.222)
shift	0.883 (0.0368)	1.492 (0.756)
shift+mondrian	0.905 (0.0222)	2.816 (0.971)

d_{BC} (simulated data)	coverage	size
all	0.9 (0.0136)	0.902 (0.297)
mondrian	0.922 (0.0111)	1.622 (0.604)
shift	0.888 (0.017)	0.891 (0.445)
shift+mondrian	0.905 (0.022)	1.413 (0.568)

d_{TV} (simulated data)	coverage	size
all	0.911 (0.032)	0.934 (0.070)
mondrian	0.988 (0.0136)	1.004 (0.035)
shift	0.922 (0.040)	0.851 (0.127)
shift+mondrian	0.961 (0.013)	0.870 (0.071)

Table 1: Coverage and size of the CP upper bound on simulated data. The KL, BC, and TV divergences were estimated using the empirical approximation of Section 2.3 with the Logistic Regression density-ratio estimator described in Section 3.2. The reported values are the means and standard deviations of 5 leave-one-out runs obtained by removing one machine from all data sets.

d_{KL} (real data)	coverage	size
all	0.787 (0.063)	0.104 (0.007)
mondrian	0.987 (0.024)	0.156 (0.004)
shift	0.725 (0.151)	0.102 (0.017)
shift+mondrian	0.962 (0.049)	0.161 (0.011)

d_{BC} (real data)	coverage	size
all	0.837 (0.084)	0.031 (0.001)
mondrian	0.887 (0.061)	0.0356 (0.001)
shift	0.750 (0.142)	0.0275 (0.003)
shift+mondrian	0.925 (0.072)	0.040 (0.004)

d_{TV} (real data)	coverage	size
all	0.775 (0.093)	0.395 (0.0107)
mondrian	1.000 (0.000)	0.562 (0.0154)
shift	0.600 (0.108)	0.372 (0.041)
shift+mondrian	0.912 (0.050)	0.503 (0.009)

Table 2: Coverage and size of the CP upper bounds for the real-data experiment described in Section 3.5. The reported values are the mean and standard deviation of 5 leave-one-out runs, each one obtained by removing the data from one of the 5 quantum machines

and d_{BC} may come from the choice of factorizable Bernoulli distributions. Remarkably, the ratio estimation remains good when the dimensionality of the support increases exponentially (from $s = 10$ to $s = 80$).

Simulated data The nearly perfect coverage of `all` is probably due to the 5-fold larger calibration set but suggests that the (simulated) noise distribution is exchangeable across different circuit sizes. `shift` produced more efficient prediction intervals overall but undercovered in some cases. `mondrian` was the less efficient on these simulations but improved after combining it with a trained shift model, as in `shift+mondrian`.

Real data The consistent undercoverage of `all` shows that noise distributions are more affected by changing a circuit’s depth than size. The performance in the four different setups followed the same pattern as for simulated data. `shift` serious low validity was likely due to the reduced size of the training data set.⁴ Except for d_{TV} , where `shift+mondrian` was the best model, the performance of `mondrian` and `shift+mondrian` was comparable.

Impact Statement

This paper presents work whose goal is to advance the field of Machine Learning and Quantum Computing. There are many potential societal consequences of our work, none of which we feel must be specifically highlighted here.

References

- Adeniyi, T. B. and Kumar, S. A. (2025). Adaptive neural network for quantum error mitigation. *Quantum Machine Intelligence*, 7(1):1–14.
- Angelopoulos, A. N. and Bates, S. (2021). A gentle introduction to conformal prediction and distribution-free uncertainty quantification. *arXiv preprint arXiv:2107.07511*.
- Anthony, B. (2020). Constructing normalized nonconformity measures based on maximizing predictive efficiency.

⁴The test Error Rate of g was high on average (data not shown).

- Apak, B., Bandic, M., Sarkar, A., and Feld, S. (2024). Ketgpt - dataset augmentation of quantum circuits using transformers.
- Arute, F., Arya, K., Babbush, R., Bacon, D., Bardin, J. C., Barends, R., Biswas, R., Boixo, S., Brandao, F. G., Buell, D. A., et al. (2019). Quantum supremacy using a programmable superconducting processor. *Nature*, 574(7779):505–510.
- Barber, R. F., Candes, E. J., Ramdas, A., and Tibshirani, R. J. (2023). Conformal prediction beyond exchangeability. *The Annals of Statistics*, 51(2):816–845.
- Barenco, A., Bennett, C. H., Cleve, R., DiVincenzo, D. P., Margolus, N., Shor, P., Sleator, T., Smolin, J. A., and Weinfurter, H. (1995). Elementary gates for quantum computation. *Physical review A*, 52(5):3457.
- Belhasin, O., Romano, Y., Freedman, D., Rivlin, E., and Elad, M. (2023). Principal uncertainty quantification with spatial correlation for image restoration problems. *IEEE Transactions on Pattern Analysis and Machine Intelligence*.
- Bhattacharyya, A. (1946). On a measure of divergence between two multinomial populations. *Sankhyā: the indian journal of statistics*, pages 401–406.
- Boström, H. and Johansson, U. (2020). Mondrian conformal regressors. In *Conformal and Probabilistic Prediction and Applications*, pages 114–133. PMLR.
- Buriticá, G. and Engelke, S. (2024). Progression: an extrapolation principle for regression. *arXiv preprint arXiv:2410.23246*.
- Cai, Z., Babbush, R., Benjamin, S. C., Endo, S., Huggins, W. J., Li, Y., McClean, J. R., and O’Brien, T. E. (2023). Quantum error mitigation. *Reviews of Modern Physics*, 95(4):045005.
- Campos, M., Farinhas, A., Zerva, C., Figueiredo, M. A., and Martins, A. F. (2024). Conformal prediction for natural language processing: A survey. *Transactions of the Association for Computational Linguistics*, 12:1497–1516.

- Canonici, E., Martina, S., Mengoni, R., Ottaviani, D., and Caruso, F. (2024). Machine learning based noise characterization and correction on neutral atoms nisq devices. *Advanced Quantum Technologies*, 7(1):2300192.
- Caro, M. C., Huang, H.-Y., Cerezo, M., Sharma, K., Sornborger, A., Cincio, L., and Coles, P. J. (2022). Generalization in quantum machine learning from few training data. *Nature communications*, 13(1):4919.
- Colombo, N. (2024). Normalizing flows for conformal regression. In *Proceedings of the Fortieth Conference on Uncertainty in Artificial Intelligence*, pages 881–893.
- Colombo, N. and Vovk, V. (2020). Training conformal predictors.
- Dasgupta, S. and Humble, T. S. (2022). Assessing the stability of noisy quantum computation. In *Quantum Communications and Quantum Imaging XX*, volume 12238, pages 44–49. SPIE.
- DeCross, M., Haghshenas, R., Liu, M., Rinaldi, E., Gray, J., Alexeev, Y., Baldwin, C. H., Bartolotta, J. P., Bohn, M., Chertkov, E., Cline, J., Colina, J., DelVento, D., Dreiling, J. M., Foltz, C., Gaebler, J. P., Gatterman, T. M., Gilbreth, C. N., Giles, J., Gresh, D., Hall, A., Hankin, A., Hansen, A., Hewitt, N., Hoffman, I., Holliman, C., Hutson, R. B., Jacobs, T., Johansen, J., Lee, P. J., Lehman, E., Lucchetti, D., Lykov, D., Madjarov, I. S., Mathewson, B., Mayer, K., Mills, M., Niroula, P., Pino, J. M., Roman, C., Schechter, M., Siegfried, P. E., Tiemann, B. G., Volin, C., Walker, J., Shaydulin, R., Pistoia, M., Moses, S. A., Hayes, D., Neyenhuis, B., Stutz, R. P., and Foss-Feig, M. (2024). The computational power of random quantum circuits in arbitrary geometries.
- Devroye, L., Mehrabian, A., and Reddad, T. (2018). The total variation distance between high-dimensional gaussians with the same mean. *arXiv preprint arXiv:1810.08693*.
- Dunn, R., Wasserman, L., and Ramdas, A. (2018). Distribution-free prediction sets with random effects. *arXiv preprint arXiv:1809.07441*.
- Feynman, R. P. et al. (1951). The concept of probability in quantum mechanics. In *Proceedings of the Second Berkeley Symposium on Mathematical Statistics and Probability*, volume 533.

- Ghosal, R. and Matabuena, M. (2023). Multivariate scalar on multidimensional distribution regression. *arXiv preprint arXiv:2310.10494*.
- Gibbs, I. and Candes, E. (2021). Adaptive conformal inference under distribution shift. *Advances in Neural Information Processing Systems*, 34:1660–1672.
- Google (2023). Suppressing quantum errors by scaling a surface code logical qubit. *Nature*, 614(7949):676–681.
- Gretton, A., Borgwardt, K. M., Rasch, M. J., Schölkopf, B., and Smola, A. (2012). A kernel two-sample test. *The Journal of Machine Learning Research*, 13(1):723–773.
- Guan, L. (2023). Localized conformal prediction: A generalized inference framework for conformal prediction. *Biometrika*, 110(1):33–50.
- Harper, R., Flammia, S. T., and Wallman, J. J. (2020). Efficient learning of quantum noise. *Nature Physics*, 16(12):1184–1188.
- Hu, X. and Lei, J. (2024). A two-sample conditional distribution test using conformal prediction and weighted rank sum. *Journal of the American Statistical Association*, 119(546):1136–1154.
- IBM (2025). Quantum processing units. *Quantum*.
- Kutiél, G., Cohen, R., Elad, M., Freedman, D., and Rivlin, E. (2023). Conformal prediction masks: Visualizing uncertainty in medical imaging. In *International Workshop on Trustworthy Machine Learning for Healthcare*, pages 163–176. Springer.
- Lidar, D. A. and Brun, T. A. (2013). *Quantum error correction*. Cambridge university press.
- Liu, J. and Zhou, H. (2020). Reliability modeling of nisq-era quantum computers. In *2020 IEEE international symposium on workload characterization (IISWC)*, pages 94–105. IEEE.
- Martina, S., Buffoni, L., Gherardini, S., and Caruso, F. (2022). Learning the noise fingerprint of quantum devices. *Quantum Machine Intelligence*, 4(1):8.

- McEwen, M., Faoro, L., Arya, K., Dunsworth, A., Huang, T., Kim, S., Burkett, B., Fowler, A., Arute, F., Bardin, J. C., et al. (2022). Resolving catastrophic error bursts from cosmic rays in large arrays of superconducting qubits. *Nature Physics*, 18(1):107–111.
- Messoudi, S., Destercke, S., and Rousseau, S. (2021). Copula-based conformal prediction for multi-target regression. *Pattern Recognition*, 120:108101.
- Nguyen, T., Lyakh, D., Dumitrescu, E., Clark, D., Larkin, J., and McCaskey, A. (2021). Tensor network quantum virtual machine for simulating quantum circuits at exascale.
- Papadopoulos, H., Gammerman, A., and Vovk, V. (2008). Normalized non-conformity measures for regression conformal prediction. In *Proceedings of the IASTED International Conference on Artificial Intelligence and Applications (AIA 2008)*, pages 64–69.
- Park, S. and Simeone, O. (2023). Quantum conformal prediction for reliable uncertainty quantification in quantum machine learning. *IEEE Transactions on Quantum Engineering*.
- Patra, S., Jahromi, S. S., Singh, S., and Orús, R. (2024). Efficient tensor network simulation of ibm’s largest quantum processors. *Physical Review Research*, 6(1):013326.
- Preskill, J. (2012). Quantum computing and the entanglement frontier.
- Qiskit (2025). aersimulator. *Python*.
- Rajeev, A. e. a. (2024). Quantum error correction below the surface code threshold.
- Sason, I. (2015). On reverse pinsker inequalities. *arXiv preprint arXiv:1503.07118*.
- Smirnov, N. V. (1939). On the estimation of the discrepancy between empirical curves of distribution for two independent samples. *Bull. Math. Univ. Moscou*, 2(2):3–14.
- Strikis, A., Qin, D., Chen, Y., Benjamin, S. C., and Li, Y. (2021). Learning-based quantum error mitigation. *PRX Quantum*, 2(4):040330.

- Stutz, D., Cemgil, A. T., Doucet, A., et al. (2021). Learning optimal conformal classifiers. *arXiv preprint arXiv:2110.09192*.
- Sugiyama, M., Suzuki, T., and Kanamori, T. (2012). *Density ratio estimation in machine learning*. Cambridge University Press.
- Thorbeck, T., Eddins, A., Lauer, I., McClure, D. T., and Carroll, M. (2023). Two-level-system dynamics in a superconducting qubit due to background ionizing radiation. *PRX Quantum*, 4(2):020356.
- Tibshirani, R. J., Foygel Barber, R., Candès, E., and Ramdas, A. (2019). Conformal prediction under covariate shift. *Advances in neural information processing systems*, 32.
- Tindall, J., Fishman, M., Stoudenmire, E. M., and Sels, D. (2024). Efficient tensor network simulation of ibm’s eagle kicked ising experiment. *Prx quantum*, 5(1):010308.
- Van Den Berg, E., Mineev, Z. K., Kandala, A., and Temme, K. (2023). Probabilistic error cancellation with sparse pauli–lindblad models on noisy quantum processors. *Nature physics*, 19(8):1116–1121.
- Vovk, V. (2012). Conditional validity of inductive conformal predictors. In *Asian conference on machine learning*, pages 475–490. PMLR.
- Vovk, V., Gammerman, A., and Shafer, G. (2005). *Algorithmic learning in a random world*, volume 29. Springer.
- Wang, Z., Gao, R., Yin, M., Zhou, M., and Blei, D. M. (2022). Probabilistic conformal prediction using conditional random samples. *arXiv preprint arXiv:2206.06584*.
- Zheng, M., Li, A., Terlaky, T., and Yang, X. (2023). A bayesian approach for characterizing and mitigating gate and measurement errors. *ACM Transactions on Quantum Computing*, 4(2):1–21.